Interactions of a Single Ink jet Drop with Well-Characterized Surfaces

*H. Park, W.W. Carr, and J. Zhu**
School of Textile and Fiber Engineering, Georgia Institute of Technology
**Institute of Paper Science and Technology*
Atlanta, Georgia

Abstract

A comprehensive study on the interactions of a single ink jet drop impacting on well-characterized surfaces at room temperature were studied. The effects of several parameters (kinetic energy, solid-liquid interactions, and energy dissipation) on spreading and retracting were investigated. Textile-like rough surfaces were compared with flat surfaces, and the effect of impact position on the rough surface was also investigated.

Introduction

The impacting and spreading of liquid drops on solid surfaces are scientifically and practically important in many applications such as spray coating, delivery of agricultural chemicals, spray painting, as well as ink jet printing.

Worthington[1] reported an investigation of drops of liquids falling vertically on a horizontal plate in 1877. Since then, there have been a number of investigations; however, a complete understanding of the phenomenon is yet to be achieved. While some of the investigations have been entirely experimental,[1-3] most of the studies have included theoretical and/or numerical modeling approaches for predicting the spreading phenomenon. The theoretical approach[4-10] involves the use of an energy balance on the system that consists of the drop and the surfaces to develop an equation for predicting spreading ratio (contact diameter to initial drop diameter) as a function of drop properties and dynamic contact angle. Numerical modeling[9,11-13] has been used to simulate the dynamics of transient flow and to predict spreading ratio during the drop impacting process.

Because fundamental understanding of the fluid dynamics associated with drop impingement is important for the overall process development and further advancement of understanding ink jet printing quality on textiles,[14] a comprehensive experimental study on the impaction of a single ink jet drop on well-characterized surfaces was carried out., The research was conducted using single-phase drops. The effects of several parameters (kinetic energy, solid-liquid interactions, and energy dissipation) on spreading and retracting are discussed. Observations of a drop impacting textile-like rough surfaces are also reported.

Experimental

Materials

The liquids used in the tests were distilled water, n-Octane, n-Tetradecane, and n-Hexadecane (Aldrich). A Brookfield viscometer (model DV-1) was used to measure the viscosity of the fluid. A Bubble Pressure Tensiometer (BP2 Kr•ss GmbH) was used to measure dynamic surface tension. The surface tensions, viscosities, and densities of three materials are given in Table 1.

Four surfaces were used in the tests. One was an uncoated silicon wafer, and the second was a silicon wafer coated with 1,1,1,3,3,3, Hexamethyl disilazane (HMDS, Aldrich). The coating was applied using a CEE Model 100CB Spinner. The third was a slide glass (Fisher Scientific), and the fourth was Teflon coated aluminum film (Bytac® Teflon® Surface Protectors). The glass and Teflon surfaces are highly hydrophilic and hydrophobic surfaces, respectively. Contact angles of liquids on several substrates were measured using a VCA2500KE Contact Angle Surface Analysis System, and the results are shown in Tables 2 and 3.

Table 1. Properties of three liquids used in tests

	Viscosity (mPa·s)	Density (10^3kg/m^3)*	Surface Tension (mN/m)
Distilled water	1.0	1.0	73
n-Octane	0.54	0.703	22
n-Tetradecane	2.17	0.763	26
n-Hexadecane	3.34	0.773	30

*Data from reference 15.

Table 2. Contact angles of distilled water on various surfaces.

	Teflon film	HMDS coated silicon wafer	Uncoated silicon wafer	Slide glass
Contact angle (degrees)	113	73	33	31

Table 3. Contact angles of n-Octane and n-Hexadecane with various surfaces

		Teflon film	HMDS coated silicon wafer	Uncoated silicon wafer
Contact angle (degrees)	n-Octane	31	0	0
	n-Hexadecane	50	0	0

A rough surface was produced by aligning and gluing polyester monofilaments coated with ethylene tetra-fluoride on a silicon wafer. The roughness was characterized by amplitude and wavelength (texture) which are 1.25 and 13mm, respectively.

Apparatus

Two experimental setups were used for the drop impingement tests. For both set ups, a syringe pump (Model 230; KD Scientific Corp.) connected to a flat-tipped stainless steel needle (28G) was used to generate a single drop on demand. The needle of the syringe pump was set vertically.

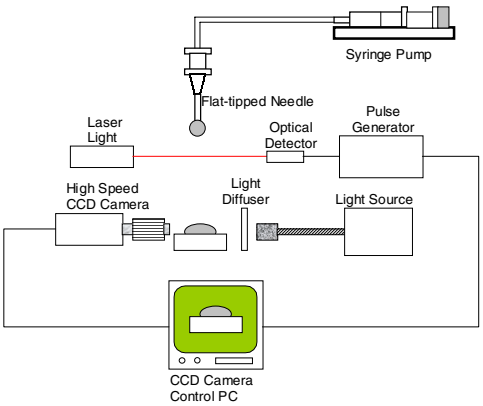

Figure 1. Experimental setup of a single-drop apparatus using SensiCam.

In the first setup as shown in Figure 1, an in-house made optical trigger consisting of a detector (OPTOLOGIC^{tm} QSA157, Fairchild semiconductor) and a laser light source. The trigger can detect a falling drop when it passed through the laser light and sends a 5-volt TTL signal to a high-speed CCD camera, (SensiCam the COOKE Corporation, Auburn Hills, MI), after a preset time delay. The settings of the CCD camera were 100 μs exposure time 800×600 spatial resolution, and 8 bit gray scale in black and white. The camera captures images of the impinging drop and loads the digital file in a computer. Replicate experiments of single drop impingement were conducted to reproduce the entire drop impingement event using different time delays of the CCD camera. The high-speed CCD camera was also used to determine drop diameter and drop speed when double exposures were superimposed in one frame.

A Kodak MotionCorder Analyzer (Eastman Kodak Company, Model 1000) was used to take continuous pictures of a single event. A series of pictures were recorded from one drop impingement event using a camera recording speed 3000fps. Other settings of the camera were 200 μs exposure time, 128x96 spatial resolution, and 8 bit gray scale in black and white. Drop impacting speed was measured via counting pixels between two different frames before impacting.

The Kodak camera is capable of recording the entire event in one experiment, but has a lower spatial resolution than the Sensicam camera. Therefore, the Sensican was used in experiments with the rough textile like surface where spatial resolution is important for accuracy

Results and Discussion

Drop spreading ratio (D/d), the diameter of the liquid-solid interface to the diameter of the impacting drop, is used to analyze the impact process. The effects of several parameters on D/d are discussed.

Kinetic energy is a major factor affecting the maximum spreading ratio. Experiments were performed with a Re number range of 0 to 6000. Solid-liquid interaction is another important factor. Dimensionless spreading coefficient (cos θ-1) was used to show its effect. At the low kinetic energy, the effect of the interaction is clearly observed. Dissipation energy[16] includes both viscous dissipation and liquid-surface adhesion. Work of adhesion, $\gamma_{LV}(1+\cos\theta)$ is used for explaining the dissipation by the liquid-surface interaction.

The typical stages in the spreading and retracting of a drop impacting on a horizontal smooth surface are illustrated in Figure 2 measured by the Kodak camera. The figure shows the impact spreading ratio of a 2.3mm water drop with impact speed of 1 m/sec on various surfaces at room temperature. The Re and We at this impact velocity are 2000 and 24, respectively. The images were taken at (A), t = 0.0 ms, show the spherically shaped drops just before impact. At (B), t ≈ 1.7 ms, the drops on the various surfaces were approximately at the maximum spreading ratio (D_m/d). The drop on the glass and uncoated silicon wafer surfaces did not reach their maximum spreading ratio until t ≈ 2.0 ms. The maximum spreading ratios on the glass and the silicon wafer are only about 10-20 % greater than

that on other surfaces. The surface energies of the glass and the silicon wafer are high; thus, the interactions between the distilled water and these surfaces are greater than those of the other surfaces.

After the maximum spreading ratio was reached, retracting began and spreading ratio decreased. At (C), t = 4.5 ms, the drops on the Teflon and polymer coated silicon wafer began to rise up, but did not leave the surface. At higher impact speeds, the drop rose above the Teflon surface slightly. The drops on the glass and the uncoated silicon surfaces recoiled very little.

After maximum retraction, spreading ratio increased. At (D), t = 10.0 ms, equilibrium spreading ratio was reached.

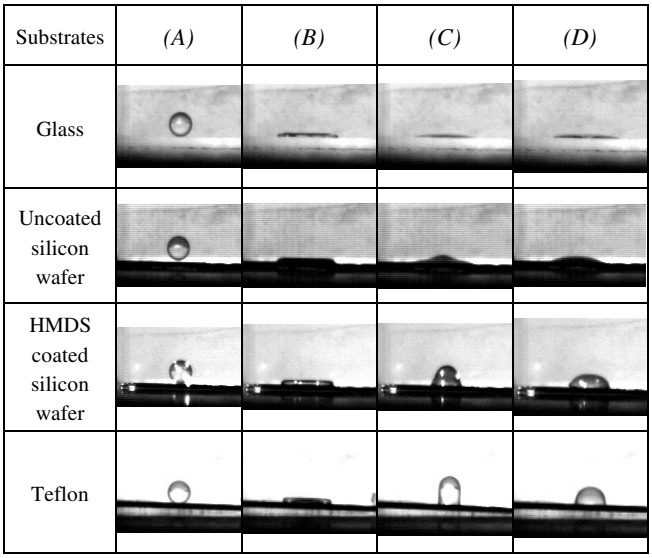

Figure 2. Spreading and retracting of a water drop impacting horizontal smooth surfaces (spreading coefficient >0).

Kinetic Energy Effects

Figure 3 shows the influence of kinetic energy on the spreading and retracting of a water drop on various surfaces. Results are shown for the following four impact velocities (kinetic energies): 0.083m/s (2.2×10^{-8} J), 0.73m/s (1.7×10^{-6} J), 1.27m/s (5.1×10^{-6} J), and 2.36m/s (1.8×10^{-5} J).

The maximum spreading ratio increases with increasing impact velocity for all of the surfaces. Figures 3(a) is for a hydrophilic surface, and the equilibrium contact angle that water makes with the surface is 31º. Figures 3(b) is for a hydrophobic surface, and the equilibrium contact angles that water makes with the surface is 113º. The impacting process for the hydrophilic surface has only two stages: spreading and retracting. After reaching the maximum spreading ratio, the drop retracts to the equilibrium spreading ratio. The impacting process for the hydrophobic surface includes spreading, retracting, rebounding, and then spreading to the equilibrium spreading ratio.

The equilibrium spreading ratio is primarily determined by the liquid-surface interaction, which is characterized by the equilibrium contact angle. It varies slightly with impact speed for the hydrophilic surfaces, but does not vary much for the hydrophobic surfaces.

The time to reach the maximum spreading ratio decreases as the impacting velocity (kinetic energy) of the drop increases**.** Dimensionless time to reach maximum spreading, $t^* = t\cdot u/d$, increases with impact velocity, rather than equal to the constant value of 8/3 predicted by Pasandideh-Fard et al.[9]

When the impact velocity approaches zero, the impact process is dominated by the interaction of the liquid and the surface, and primarily involves spreading as shown in Figure 4. After reaching the maximum spreading ratio (which is very close to the equilibrium spreading ratio), a small amount of retracting and spreading may be present, but it is too small to be detected accurately by the Kodak camera system used for this test.

Influence of Solid-liquid Interactions

A normalized spreading coefficient,

$$\frac{W_s}{\gamma_{LV}},$$

is useful in showing the influence of solid-liquid interactions on the impacting process. When a unit area of solid-vapor interface is replaced with a unit area of liquid-solid interface and a unit area of liquid-vapor interface, the change of Gibbs free energy is given by the following expressions.[17]

$$\Delta G = -S = \gamma_{LS} + \gamma_{LV} - \gamma_{SV} \tag{1}$$

where S is spreading coefficient, γ_{LS} is interfacial energy between liquid and solid, γ_{LV} is surface energy of liquid with vapor, γ_{SV} is surface energy of solid with vapor.

The normalized spreading coefficient is obtained by dividing through by γ_{LV}.

$$\frac{S}{\gamma_{LV}} = \frac{\gamma_{SV} - \gamma_{LS}}{\gamma_{LV}} - 1 \tag{2}$$

For an equilibrium contact angle $\theta > 0$, Equation (1) can be combined with Young's equation to give

$$\frac{S}{\gamma_{LV}} = \cos\theta - 1 \tag{3}$$

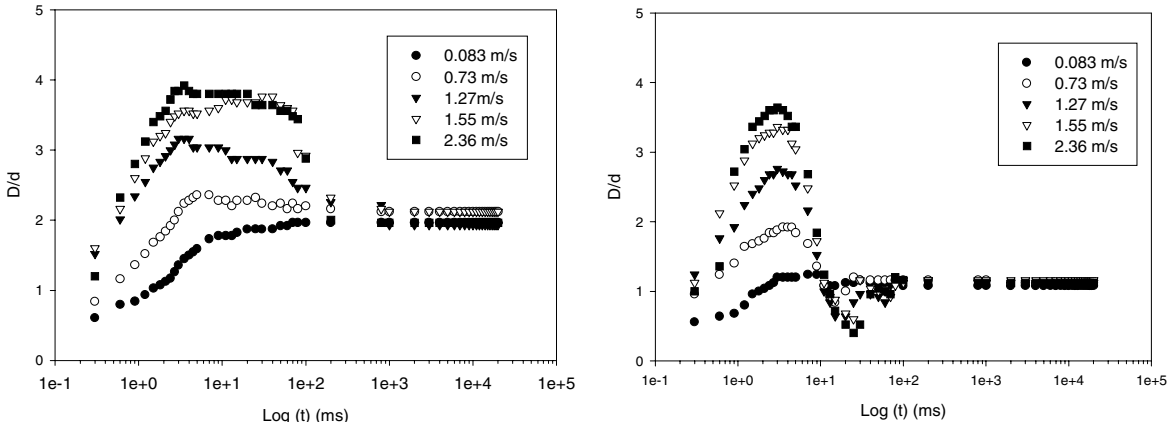

(a) *(b)*

Figure 3. Spreading and retracting of a 2.3 mm water drop on two surfaces: (a) Glass (θ =31º) and (b) Teflon (θ =113º).

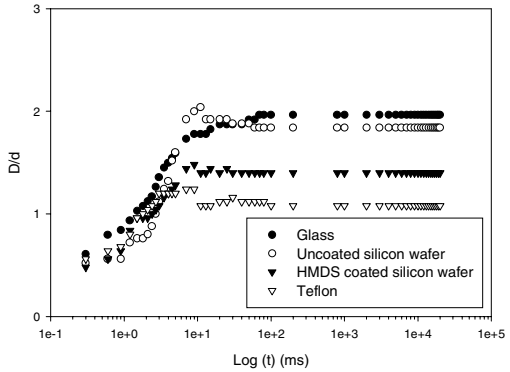

Figure 4. Spreading of a 2.3 mm water drop on various surfaces at a very low impact velocity of 0.083m/s.

Figure 5 shows the effect of normalized spreading coefficient on the maximum spreading ratio of a water drop with various impact velocities. The maximum spreading ratio increases with increasing normalized spreading coefficient. The normalized spreading coefficient increases as the equilibrium contact angle (θ) increases. The two limiting values of θ, 0 and 180º, are not shown in this figure. When θ is zero, the spreading is spontaneous, so D/d increases to very large values for all impact velocities. This is not shown in the figure, but will be discussed later. When θ is 180º, maximum spread ratio depends on impact velocity. Equilibrium spreading ratio is approximately zero when θ is 180º.

Figure 5 can be used to compare the effect of impact velocity with that of the interaction of the liquid with the solid surface. The lower curve is for a very low impact velocity (0.086 m/s). Spreading is driven almost entirely by the interaction of the liquid with the solid surface. For the surface where

$$\frac{S}{\gamma_{LV}}$$

is about -0.14, the D_m/d is about 45% greater than for the surface where

$$\frac{S}{\gamma_{LV}}$$

is about -1.39.

As impact velocity increases, D_m/d increases, and the differences in D_m/d for the various surfaces gets much smaller. At impact velocity of 2.34 m/s, the difference is only 10% between the lowest and highest values. For this case, since We is 176, kinetic energy of the impacting drop is about 14.7 times larger than the impacting drop surface energy.

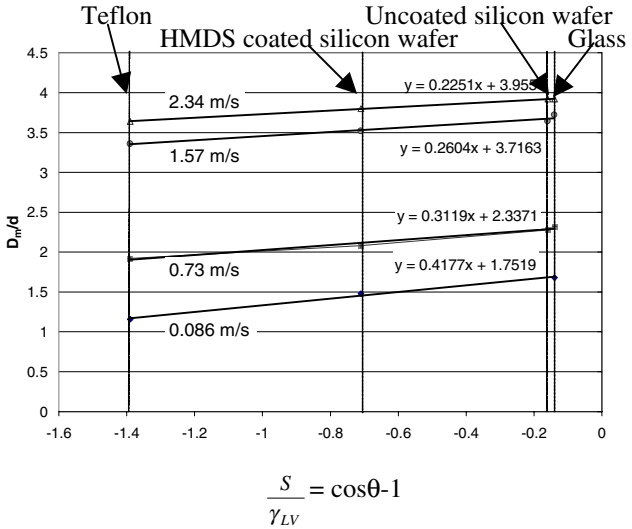

Figure 5. Effect of normalized spreading coefficient on maximum spreading ratio of water drop impacting various surfaces.

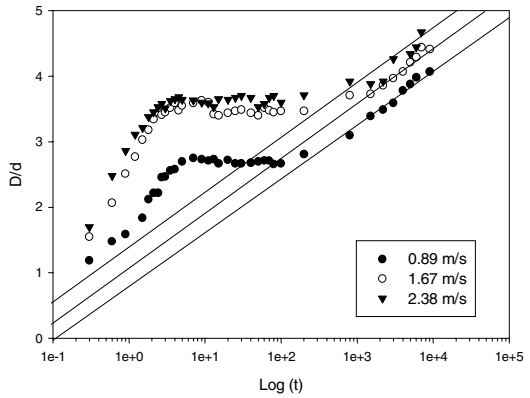

Figure 6. Impact of a 2.0 mm n-Tetradecane drop on an uncoated silicon wafer surface.

Spreading Coefficient Greater Than Zero

When spreading coefficient is greater than or equal to zero, the liquid will spontaneously spread over the surface (see Figure 6). For zero impact velocity, the variation of spreading ratio with time is well fitted by a power-law relationship.[18,19] For impact velocity greater than zero, there is an initial period where the spreading is driven by the kinetic energy of the impacting drop, and the spreading ratio increase much faster than that for the zero impact velocity case. After the initial rapid spreading period, the spreading ratio is almost constant for a period of time. Then spontaneous spreading begins, and the variation of spreading ratio with time is well fitted by a power-law relationship as shown**.**

Energy Dissipation

Kinetic and surface energies are dissipated during the impact process. De Gennes[22] discusses several types of dissipative processes that can occur during spreading of a liquid. The dissipative processes can occur in the following three locations: 1) the wedge of fluid behind the contact line, 2) the extremely thin (submicron thickness) precursor film which shows up ahead of the nominal contact line, and 3) region in the close vicinity of the real contact line. Mechanisms for the dissipation processes are not completely understood.

The influence of viscosity on the spreading ratio of an alkane drop on a Teflon surface can be seen in Figure 7. Experiments were performed holding Weber number nearly constant (158 for n-Octane and 160 for n-Hexadecane) while Reynolds number was different (4087 for n-Octane and 856 for n-Hexadecane). Spreading ratio was nearly the same during the early stages of spreading ($t < 1ms$, $t^* \approx 0.85$). The maximum spreading ratio of the n-Hexadecane drop is about 77% of that of the n-Octane drop even though its impact kinetic energy is about 50% greater than that of the n-Octane. This illustrates the effect of energy dissipation due to viscosity. The viscosity of the n-Hexadecane is about 6.2 times greater than for n-Octane.

Figure 8 shows the spreading ratio of a water drop impacting four different smooth surfaces. Since the impact velocity and drop diameter were held nearly constant, the Reynolds and Weber numbers are almost identical for the four experiments, i.e., 3003 and 53, respectively. Thus the major difference is the liquid surface interactions, which are characterized by the equilibrium contact angles (see Table 2). Kinetic energy of the impacting drop dominates during the first stage of spreading, and the spreading ratio is almost identical until the maximum spreading ratio is approached. The maximum spreading ratio is slightly higher for the glass, as expected, since the spreading coefficient is highest for water on glass.

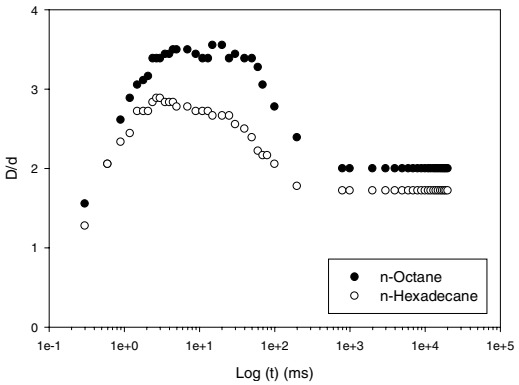

Figure 7. Spreading of 2mm alkane drops on a Teflon surface. Re of 4087 (n-Octane) and 856 (n-Hexadecane), and We of 158 (n-Octane) and 160 (n-Hexadecane).

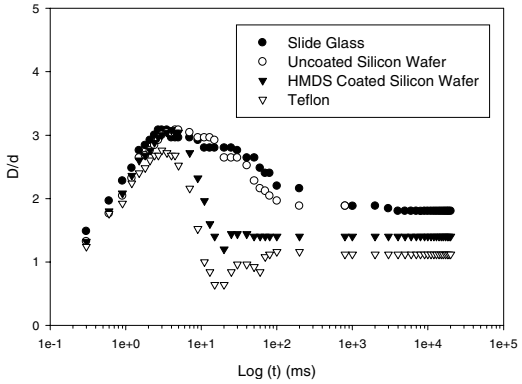

Figure 8. Impact of a 2.3 mm water drop on the various surfaces at 1.27m/s. Re =3003, We = 53.

At maximum spreading ratio, the energy in the drop surface is greater than for the equilibrium spreading ratio. As a result, the contact angle decreases below its equilibrium value and the spreading ratio decreases. Since water is used for the four experiments, viscosity is the same for the four experiments. However, spreading behavior on the four surfaces is quite different. The drop retracts much more slowly on the glass and uncoated silicon wafer, and does not retract as far. The drops on the HMDS coated silicon wafer and Teflon not only retract much faster, but

retract through the equilibrium position, sometimes rebound, and then spread back to the equilibrium position.

Since viscosity is the same in the four experiments, the difference in the behavior after the drop reaches maximum spread must be explain by some other factor. This is explained by the differences in the liquid surface interaction. When the droplet retracts, the liquid is removed from the solid surface. The energy required to remove the liquid depends on the affinity of the liquid for the surface, which is characterized the work of adhesion, which is equal to γ_{LV} (1 + cos θ). The smaller θ, the larger the amount of energy to remove the liquid. Thus as the drop retracts more of the energy stored in the liquid surface is consumed in removing the liquid, and less is available to be converting into kinetic energy.

Effect of Rough Surface

The spreading of a water drop on a rough surface is compared with the spreading on a smooth surface in Figure 9. The rough surface was produced to simulate a typical fabric surface such as shown in Figure 10.

The impacting process was studied with the drop impacting the rough surface at three locations. One is in the center of the filament-like structure. The second is in the middle of the valley between two of the filament-like structures. The third is somewhere between the positions of the drops in first and second positions. A series of images of drop impingement for the three impact positions and the smooth surface are recorded using almost identical time steps.

Much of the drop liquid flowed in the filament axial direction because of barriers in the radial direction. The spreading and retracting shapes and maximum spreading ratios depend on the impact position. Maximum spreading ratio in the radial direction was the largest for impact position 2 while the maximum spreading ratio in the axial direction was the largest for position 1. The equilibrium diameter in the radial direction for position 2 and 3 are bigger than for position 1 due to the barriers in radial direction. However, the equilibrium diameter for position 2 and 3 are almost same.

Conclusion

Research was conducted to better understand impacting and spreading of a liquid drop on various surfaces including rough surfaces, and heterogeneous surfaces at room temperature. This paper clearly shows the influence of kinetic energy, solid-liquid interactions during impact and the effects of energy dissipation. Also rough surface was considered to understand impacting on textile-like surface. The impacting process and the drop resting position depend on impact location on the rough surface.

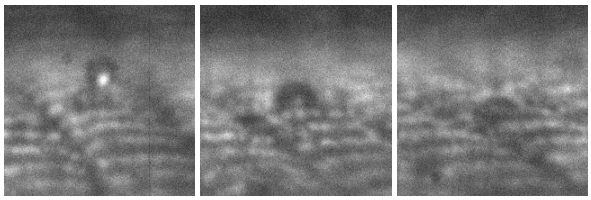

(1) (2) (3)

Figure 9. Impact of a ink jet water drop on the rayon fabric[20].

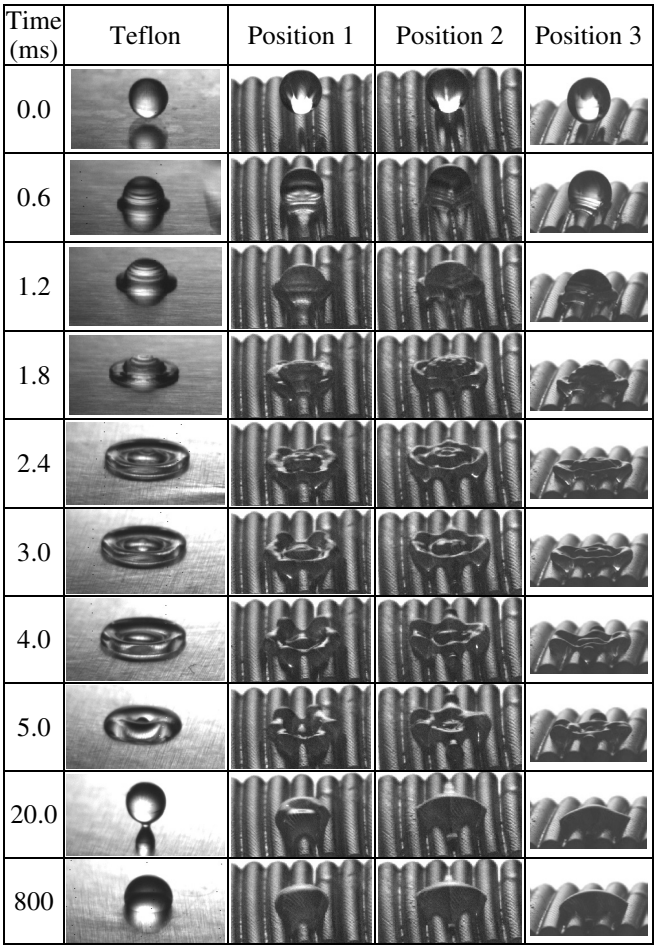

Figure 10. Impact of a 2.3 mm water drop on a rough surface produced by aligning and gluing polyester monofilaments coated with ethylene tetra-fluoride on a silicon wafer. Amplitude and texture of roughness: 1.25 and 13mm, respectively. Re = 2004, We = 24.

References

1. A. M. Worthington, *Proc. R. Soc. Lond.*, **25**, 261 (1877).
2. V. Bergeron, D. Bonn, J. Y. Martin, and L. Vovelle, *Nature*, **405**, 772 (2000).
3. Š. Šikalo, M. Marengo, C. Tropea, and E. N. Ganić, *Experimental Thermal and Fluid Science*, **25**, 503 (2002).
4. O. G. Engel, *J. Res. Natn. Bur. Stand.*, **54**, 281 (1955).

5. R. E. Ford and C. G. L. Furmidge, *Wetting. Soc. Chem. Industry Monograph*, 417 (1967).
6. A. Asai, M. Shioya, S. Hirasawa, and T. Okazaki, *J. Imaging. Sci. and Technol*., **37**, 205 (1993).
7. J. Fukai, Y. Shiiba, T. Yamamoto, O. Miyataka, D. Poulikakos, C. M. Megaridis, and Z. Zhao, *Phys. Fluids*, **7**, 236 (1995).
8. J. Fukai, M. Tanaka, and O. Miyatake, *J. Chem. Eng. Japan*, **31**, 456 (1998).
9. M. Pasandideh-Fard, Y. M. Qiao, S. Chandra, and J. Mostaghimi, *Phys. Fluids*, **8**, 650 (1996).
10. T. Mao, D. C. S. Kuhn, and H. Tran, *AIChE J.*, **43**, 2169 (1997).
11. F. H. Harlow and J. P. Shannon, *J. Appl. Phys.*, 38, 3855 (1967).
12. M. R. Davidson, *Chem. Eng. Sci.*, **55**, 1159 (2000).
13. M. Bussmann, J. Mostaghimi, and S. Chandra, *Phys. Fluids*, **11**, 1406 (1999).
14. W. W. Carr, J. F. Morris, F. J. Schork, W.C. Tincher, and J. Zhu, *NTC Annual Report C99-G08*, pg. 1 (2001).
15. CRC Press, *Handbook of Chemistry and Physics*, 6-102 (1977).
16. P. G. de Gennes, *Rev. Mod. Phys.*, **57**, 827 (1985).
17. A. W. Adamson and A.P. Gast, *Physical Chemistry of Surface*, John Willey & Sons, Inc., New York, NW, 1997, pg. 26.
18. A. Marmur, *J. Colloid Interface Sci*. **124**, 301 (1988).
19. C. M. Lin, R. M. Ybarra, and P. Neogi, *Adv. Colloid Interface Sci.,* **67**, 185 (1996).
20. H. Park, W. W. Carr, and J. Zhu, *NIP17: International Conference on Digital Printing Technologies*, 438 (2001).

Biography

Heungsup Park received his B.S. (1994) and M.S. (1996) in Textile Engineering from Pusan National University in Korea. He has also earned an M.S. in Textile Chemistry from Georgia Institute of Technology in 1999. He is currently pursuing a Ph.D. in Textile Chemistry at Georgia Institute of Technology. Mr. Park's research interests are in surface science, computational fluids and digital printing.